Combined Experimental and Theoretical Study to Understand the Photoluminescence of $Sr_{1-x}TiO_{3-x}$

Emmanuelle Orhan,*,† Fenelon M. Pontes,‡ Marcos A. Santos,‡ Edson R. Leite,‡ Armando Beltrán,§ Juan Andrés,§ Tania M. Boschi,|| Paulo S. Pizani,|| Jose A. Varela,† Carlton A. Taft,*,⊥ and Elson Longo‡

Instituto de Química, Universidade Estadual Paulista, 14801-907, Araraquara, SP, Brazil, Departamento de Química, Universidade Federal de São Carlos, 13565-905 São Carlos, SP, Brazil, Departament de Ciéncies Experimentals, Universitat Jaume I, P.O. Box 6029 AP, 12080 Castelló, Spain, Departamento de Física, Universidade Federal de São Carlos, Caixa Postal 676, 13565-905, São Carlos, SP, Brazil, and Centro Brasileiro de Pesquisas Físicas, Rua Dr. Xavier Sigaud, 150, Urca 22290-180, Rio de Janeiro, Brazil

Received: March 13, 2004; In Final Form: April 27, 2004

A joint experimental and theoretical study has been carried out to rationalize the results of visible photoluminescence measurements at room temperature on $Sr_{1-x}TiO_{3-x}$ (ST) perovskite thin films. From the experimental side, ST thin films, $x = 0$ to 0.9, have been synthesized following soft chemical processing, and the corresponding photoluminescence properties have been measured. First principles quantum mechanical techniques, based on density functional theory at the B3LYP level, have been employed to study the electronic structure of a crystalline, stoichiometric ($x = 0$) **ST-s** model and a nonstoichiometric (SrO-deficient, $x \neq 0$) and structurally disordered **ST-d** model. The relevance of the present theoretical and experimental results of the photoluminescence behavior of ST is discussed. The optical spectra and the calculations indicate that the symmetry-breaking process on going from **ST-s** to **ST-d** creates electronic levels in the valence band. Moreover, an analysis of the Mulliken charge distribution reveals a charge gradient in the structure. These combined effects seem to be responsible for the photoluminescence behavior of deficient $Sr_{1-x}TiO_{3-x}$.

I. Introduction

Visible photoluminescence (PL) at room temperature in disordered materials was first observed by Canham in porous silicon.[1] Since then, the study of PL in disordered or nanostructured materials has focused on the development of new electroluminescent materials because of their potential technological applications, which include flat-screen full-color displays. Intense visible PL at room temperature has recently been reported by our group for structurally disordered perovskite titanates $ATiO_3$ where A = Pb, Ca, Sr, and Ba.[2−15] They were synthesized by a soft chemical process called the polymeric precursor method,[16,17] a simple water-based technique allowing structurally disordered titanates to be processed at temperatures as high as 523 K in the form of thin films or powders.

Over the last 25 years, various hypotheses were proposed to explain the PL phenomenon in crystalline or disordered titanate compounds. There is a general consensus on the fact that PL emission is the result of a radiative decay of the excited electrons to the ground state. In the case of a nonradiative return to the ground states, the energy of the excited states is used to excite the vibrations of the host lattice, that is, to heat the host lattice.[18] Some authors attempt to explain how the radiative decay happens; for example, Leonelli and Brebner[19] talk about self-trapped excitons (STE), and Eglitis et al.[20] show, through semiempirical quantum chemical calculations, that the origin of the intrinsic excitonic (green) luminescence of ABO_3 perovskites at low temperature is linked to the recombination of electrons and hole polarons forming a charge-transfer vibronic exciton (CTVE).

What remains unclear is why this radiative decay occurs; that is, what are the rules allowing PL emission in the visible range in relation to temperature and lattice geometry? Bouma and Blasse[21] concluded from their extended experimental studies on titanates that compounds involving an irregular titanate octahedra with a short Ti−O distance show PL at room temperature if these octahedra are isolated from each other. They ascribed this effect to a broadening of the energy bands.

In the present paper, we are attempting to combine laboratory experiments and high-level calculations into a synergetic strategy for understanding the PL origin in $SrTiO_3$ (ST) perovskite. The experimental work presents measurements of broad, intense PL at room temperature in SrO-deficient ST thin films prepared at low temperatures by the polymeric precursor method. The aim of the theoretical part is to investigate the electronic structure of ST by using models that represent its crystalline, stoichiometric, and defective disordered structures and to give an interpretation in terms of the density of states (DOS), band-structure diagrams, and electronic density maps of the conditions allowing PL to occur at room temperature. This approach renders a plausible quantitative description of the behavior of ST under laser excitation and an interesting correlation between the theoretical and experimental results.

The paper is organized as follows: In section II, the experimental methods of the ST thin films' preparation are described, together with spectral measurement techniques.

* Corresponding authors. (C.A.T.) E-mail: taft@cbpf.br, catff@terra.com.br. (E.O.) E-mail: emmanuelle.orhan@liec.ufscar.br.
† Universidade Estadual Paulista.
‡ Departamento de Química, Universidade Federal de São Carlos.
§ Universitat Jaume I.
|| Departamento de Física, Universidade Federal de São Carlos.
⊥ Centro Brasileiro de Pesquisas Físicas.

10.1021/jp048877y CCC: $27.50
Published on Web 06/02/2004

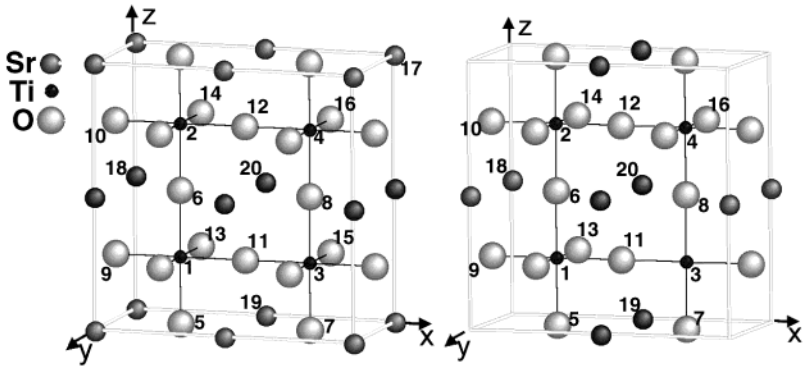

Figure 1. Supercell $2 \times 1 \times 2$ of the cubic $SrTiO_3$ unit cell without defects, stoichiometric **ST-s** (left) and after.

Section III presents the ST periodic models used for the calculations, and section IV gives the computational details. The results are discussed in an attempt to explain the PL phenomenon in section V, and section VI summarizes the main lines of our hypothesis of the origin of PL at room temperature in ST-deficient thin films.

II. Experimental Section

The polymeric precursor method was used to synthesize $Sr_{1-x}TiO_{3-x}$ ($x = 0$ to 0.9) thin films. Details of the preparation can be found in the literature.[22] The polymeric precursor solution was spin coated on substrates [Pt (140 nm)/Ti (10 nm)/SiO_2 (1000 nm)/Si] by a commercial spinner operating at 6000 rpm for 20 s (spin-coater KW-4B, Chemat Technology) via a syringe filter to avoid particulate contamination. After spinning, we put the thin films on a hot plate at 423 K in ambient air for 20 min to remove any residual solvents. The heat treatment was carried out at 623 K under oxygen flow at a heating rate of 5 K/min for 12 h to pyrolyze the organic materials. The ST thin films were structurally characterized using X-ray diffraction (XRD) (Cu Kα radiation). The diffraction patterns were recorded on a Siemens D5000 machine in a $\theta-2\theta$ configuration using a graphite monochromator; all compositions heat treated at 623 K present an amorphous diffraction pattern, with crystallization occurring only above 873 K for the stoichiometric $SrTiO_3$ thin film. The PL spectra of the ST thin films were recorded with a U1000 Jobin-Yvon double monochromator coupled to a cooled GaAs photomultiplier and a conventional photon counting system. The 488.0-nm exciting wavelength of an argon-ion laser was used, with the laser's maximum output power kept at 60 mW. A cylindrical lens was used to prevent the sample from overheating. The slit width used was 100 μm. All measurements were taken at room temperature. The spectral dependence of optical absorbance for the crystalline and disordered thin films was measured at room temperature in a Cary 5G spectrophotometer.

III. Crystal Structure and Periodic Models

Stoichiometric $SrTiO_3$ crystallizes in the well-known cubic perovskite structure (space group $Pm3m$, O_h symmetry). The strontium atoms share the vertexes of the unit cell, and the titanium is at the center of the cube, surrounded by six oxygens that occupy the middle of the faces in a regular octahedral configuration. The experimental and calculated values of the **a** parameter are, respectively, 3.90 and 3.88 Å. We have used a $2 \times 1 \times 2$ supercell to represent the cubic stoichiometric ST (**ST-s**) structure as a periodic model. It results in 20 atoms in the unit cell. Each titanium is surrounded by six oxygens in an O_h configuration. This supercell can be described as two corners sharing adjacent [TiO_6] clusters with two other adjacent [TiO_6] clusters on top of them. (See Figure 1, left.)

The XANES experimental results on the structurally disordered phase of stoichiometric $SrTiO_3$, that is, before the heat treatment leading to the phase crystallization, pointed out the coexistence of two types of environments for the titanium, namely, 5-fold oxygen−titanium coordination, square-base pyramidal [TiO_5], and 6-fold oxygen−titanium coordination [TiO_6], octahedral configuration.[15] This certain degree of order in amorphous materials was to be expected because two or more atoms arranged close to each other in a stable configuration must necessarily have some degree of order because there always are minima of the potential energy. Furthermore, as it is well-known, the details of the band structure for a periodic system is mainly determined by the potential within the unit cell rather than by the long-range periodicity. It means that any punctual deformation will have important consequences on the electronic structure. We should build a model representing the disordered thin films in which the local environment on only one titanium is perturbed to trace the effect of this perturbation on the electronic structure. Because the studied thin film is deficient in oxygen and strontium, we assume that square planar titanium environment is likely to exist.

On the basis of these results, we constructed another periodic model to represent the SrO-deficient thin films. We have removed 2 atoms from the supercell unit, Sr17 and O15, resulting in a $Sr_{0.75}TiO_{2.75}$ theoretical composition and will be designed as **ST-d**. (See Figure 1, right.) The local symmetry around Ti3 is lowered from O_h to D_{4h}. In the supercell, three [TiO_6] (O_h) clusters and a [TiO_4] (D_{4h}) cluster now coexist. The oxygen to be removed could have been either O14, O16, or O13 because they are symmetrically equivalent. However, the removal of any of the apical oxygens would have deformed the titanium environment, which is undesirable. As for the Sr atom removal, we checked all of the positions, and it did not influence the results.

The electronic structure calculated for the first periodic model, **ST-s**, stoichiometric and crystalline, will be the reference for interpreting the results obtained with the second model, **ST-d**, deficient, closer to the $Sr_{1-x}TiO_{3-x}$ ($x = 0$ to 0.9) thin films' compositions and structures.

IV. Computational Details

Calculations have been carried out with the CRYSTAL98[23] package within the framework of density functional theory (DFT) using the gradient-corrected correlation functional by Lee, Yang, and Parr, combined with the Becke3 exchange functional, B3LYP,[24,25] which has been demonstrated by Muscat et al.[26] to be suitable for calculating structural parameters and band

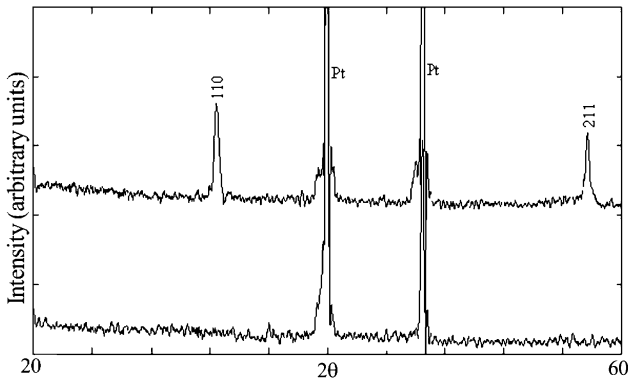

Figure 2. DRX patterns of the stoichiometric $SrTiO_3$ thin film heat treated at 873 K for 2 h (top) and of the $Sr_{0.8}TiO_{2.8}$ thin film heat treated at 623 K for 12 h (bottom), both on a Pt substrate.

structures for a wide variety of solids. The atomic centers have been described by all of the electron basis sets, 976-41(d51)G for Sr,[27] 86-411(d31)G for Ti, and 6-31G* for O.[28] The *k*-points sampling was chosen to be 40 points within the irreducible part of the Brillouin zone. To simulate the removal of the Sr17 and O15 atoms, we have used the ATOMREMO (atom removal) option provided with the CRYSTAL program. The XCrysDen program was used to design the density of states and the band structure diagrams.[29]

V. Results and Discussion

The PL reported in earlier articles[7,16] and observed in the chemically prepared structurally disordered ABO_3 (A = Sr, Ba, Pb, B = Ti, W, Mo, Zr) thin films and powders was associated with a nonuniform band-gap structure with a tail of localized states and possible mobile edges. This PL in chemically prepared ABO_3 perovskite compounds is believed to be associated with a radiative recombination between trapped electrons and holes in tail and gap states.

The diffraction patterns of two thin films, one stoichiometric, heat treated at 873 K for 2 h and the other with the $Sr_{0.8}TiO_{2.8}$ formula, heat treated at 623 K for 12 h, are presented in Figure 2. The (110) and (211) diffraction peaks of the stoichiometric thin film are clearly distinguished from the Pt substrate peaks. For the astoichiometric thin film, only the peaks related to the Pt substrate are appearing; the crystallization has not yet occurred.

The optical absorbance spectrum of the crystalline stoichiometric $SrTiO_3$ thin film is shown in Figure 3a and presents an interband transition typical of crystalline semiconducting materials. The SrO-deficient $Sr_{0.8}TiO_{2.8}$ thin film heat treated at 623 K for 12 h (Figure 3b) and the stoichiometric $SrTiO_3$ annealed at 62 3K and thus structurally disordered (Figure 3c) show a spectral dependence on absorbance similar to that of amorphous semiconductors, such as amorphous silicon (Si), and of insulators. From the Wood and Tauc method,[30] the energy band gap of the crystalline ST thin film was calculated to be 3.5 eV (Figure 3a) and is in accordance with the literature data where optical gaps of ST powders are reported to be between 3.2 and 3.4 eV.[31−35] The energy band gaps of the SrO-deficient $Sr_{0.8}TiO_{2.8}$ thin film heat treated at 623 K for 12 h and the stoichiometric $SrTiO_3$ annealed at 623 K were calculated to be 1.65 and 1.82 eV, respectively (Figure 3b and c).

In comparison to the crystalline-phase spectrum, the disordered phases' curves exhibit exponential optical edges (or Urbach edge)[36] and a typical tail in the spectral absorbance dependence (Figure 3b and c). The nature of these exponential

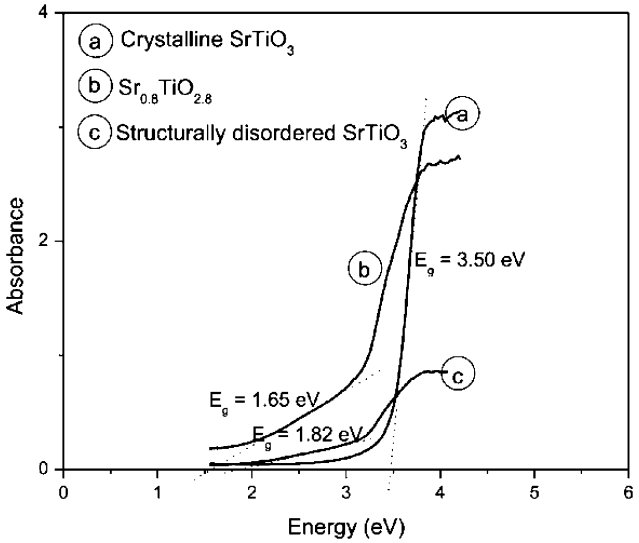

Figure 3. Spectral dependence of the absorbance for (a) a crystalline stoichiometric $SrTiO_3$ thin film, (b) a SrO-deficient $Sr_{0.8}TiO_{2.8}$ thin film, and (c) a stoichiometric structurally disordered $SrTiO_3$ thin film.

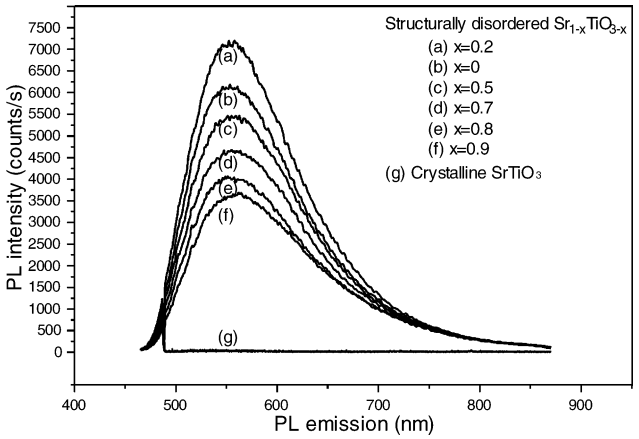

Figure 4. Photoluminescence spectra of $Sr_{1-x}TiO_{3-x}$ (x = 0 to 0.9) thin films heat treated at 623 K for 12 h and for the crystalline $SrTiO_3$ thin film heat treated at 873 K for 2 h.

optical edges and the tail may be associated with defect states promoted by the disordered structure of the thin films. The optical absorbance spectra of the other SrO-deficient thin films are not shown because they are similar to the $Sr_{0.8}TiO_{2.8}$ thin-film spectrum. The quantity of defects present in the structure does not influence the optical gap to a great extent; what is important is if the structure is disordered.

Figure 4 shows the PL spectra measured at room temperature for $Sr_{1-x}TiO_{3-x}$ (x = 0 to 0.9) thin films treated at 623 K for 12 h and for the $SrTiO_3$ crystalline thin film (annealed at 873 K for 2 h). Figure 5 presents the PL spectra's normalized intensities for a wider panel of deficient ST thin films. From $Sr_{0.1}TiO_{2.1}$ to $Sr_{0.8}TiO_{2.8}$ compositions, the measured PL intensity increases regularly. A higher concentration of SrO leads to a decrease in the PL. Twenty percent defects is thus the more efficient composition with regard to the PL properties in the ST system. For the crystalline stoichiometric thin film, no PL is measured. The wavelength used for the measurements, 488 nm, corresponds to an energy (2.54 eV) that is inferior to the energy of the band gap of the crystalline film (3.50 eV). Previous PL measurements on $LiNbO_3$ and $BaTiO_3$[16] showed a similar behavior in relation to the structural defects concentration.

To understand the relationship between the structural defects and the electronic modifications that they generate, we per-

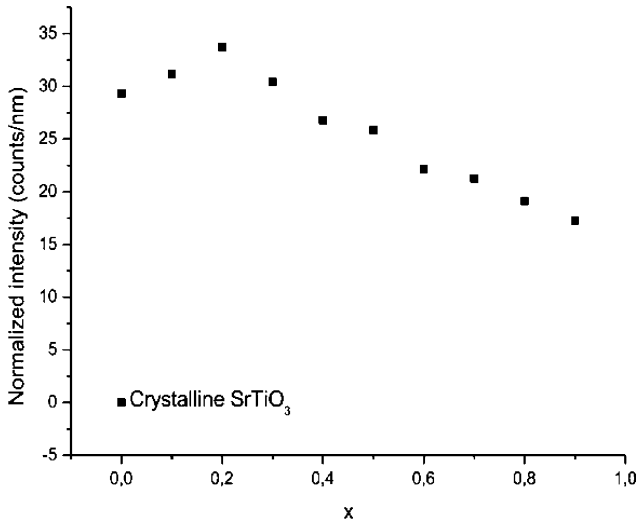

Figure 5. Photoluminescence emission maximal intensity for $Sr_{1-x}TiO_{3-x}$ ($x = 0$ to 0.9).

formed a detailed theoretical study of the electronic structure in a cubic stoichiometric **ST-s** and in an asymmetric deficient model, **ST-d**. To analyze the differences in the electronic structure, it is convenient to make reference to quantities such as the band gap or the projected DOS, which may be compared to each other independently of the crystalline space group.

The electronic structure of crystalline $SrTiO_3$ has been calculated in some previous studies at various levels. Here are some examples: Kahn and Leyendecker[37] were the first to publish their results, obtained by the linear combination of atomic orbitals (LCAO) semiempirical method. They reported a gap of about 3 eV without taking into account the Sr orbitals. About 10 years after that report, Mattheis[38] used the augmented plane wave (APW) method in combination n with the LCAO scheme to compute a gap of 2.9 eV. Mo et al.[39] used the first-principles orthogonalized LCAO method, and they found a 1.45-eV gap. These underestimations are inherent to DFT methods.[40] Heifets et al.[41] calculated a gap of 4.16 eV for $SrTiO_3$ using the hybrid Hartree−Fock DFT, B3PW functional, in the CRYSTAL98 code.

In a previous paper,[11] we reported the electronic structure of two $Sr_8Ti_3O_{12}$ clusters, one regular and one distorted, using a first-principles molecular method implemented in the Gaussian 98 code. This tool, known to superestimate the gap values, led to 4.71 and 3.99 eV, respectively, for the energy band gaps of the regular symmetric cluster and the distorted one.

In the present paper, we present the electronic structure calculation of a crystalline stoichiometric ST, **ST-s**, for comparison purposes with the **ST-d** periodic model representing SrO-deficient and structurally disordered ST.

Figure 6a shows the calculated band structure of bulk **ST-s**. The top of the valence band (VB) is at the M point and is very close to the Γ point. The bottom of the conduction band (CB) is at Γ. The minimal indirect gap between M and Γ is 3.81 eV, very close to our 3.5-eV value deduced from optical absorbance (Figure 2). The minimal direct gap at Γ is 4.02 eV.

The calculated band structure of bulk **ST-d** is depicted in Figure 6b. The top of the VB is at the R point, and the bottom of CB is at Γ, as in the case of **ST-s**. The indirect minimal gap between R and Γ is 1.0 eV, and the minimal direct gap at Γ is 1.45 eV. The indirect gap can be compared with the optical gap of the SrO-deficient thin film that we found to be 1.65 eV for the $Sr_{0.8}TiO_{2.8}$ composition (Figure 3).

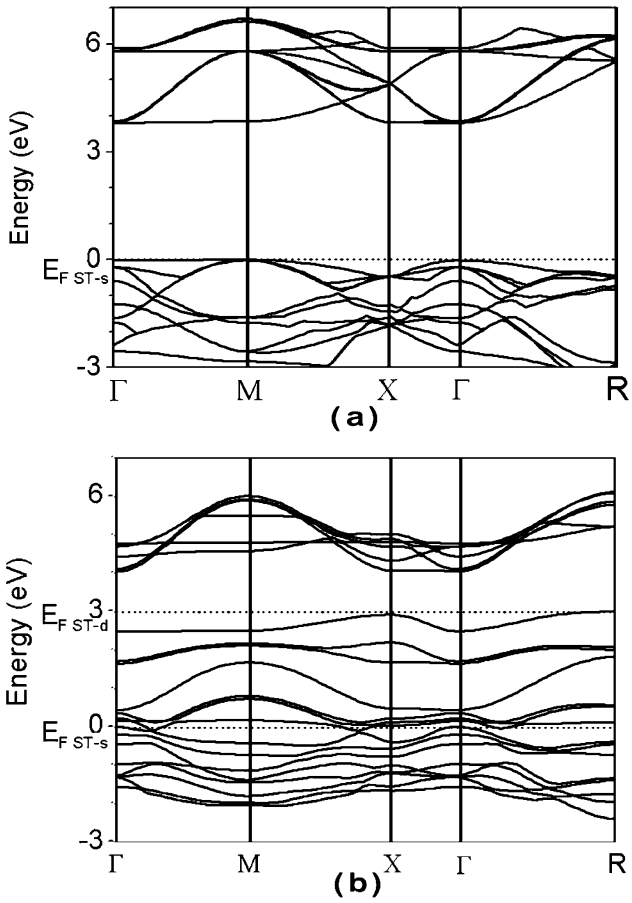

Figure 6. Band structure for **ST-s** (a) and **ST-d** (b). $E_{F_{ST-d}}$ and $E_{F_{ST-c}}$ correspond to the Fermi energies of the deficient and stoichiometric models, respectively.

The calculated total and atom-resolved projected DOS of **ST-s** and **ST-d** structures ranging from −5 below to 11 eV above the top of the **ST-s** VB are shown in Figure 7a and b, respectively. The presented curves clearly show that the VB main components are the O levels and the that CB components are the Ti levels. An analysis of the orbitals participating in each band highlighted that for **ST-s** the upper VB is predominantly made of the O (2p) states, equivalently distributed on the 12 oxygens of the structure (Figure 7a). The CB is clearly made of the Ti (3d) states with a predominant contribution of the Ti ($3d_{xy}$, $3d_{xz}$, and $3d_{yz}$) t_{2g} states at the bottom, between 4 and 5 eV, followed by Ti ($3d_{z^2-y^2}$) and ($3d_{z^2}$) character states e_g, keeping the memory of the octahedral local crystal field. The Ti−O covalent bond is traceable from the limited Ti contribution in the O region as well as from a weak O contribution to the Ti area. The Sr states, not shown in this Figure, are found between −16 and −17 eV in the case of **ST-s**. Although they show a nonnegligible hybridization with the oxygens, they are very localized, attesting to an ionic interaction.

For **ST-d** (Figure 7b), the upper VB is not dominated by O ($2p_x$, $2p_y$, and $2p_z$) character states but by the Ti3 states and more precisely by the important contribution of the $3d_{xz}$ and polarization $4d_{xz}$ orbitals of the Ti3. The analysis of the atomic Mulliken net charges shows that the Ti3 is reduced by a 0.4 e charge and that O7 and O9 are the correspondingly oxidized atoms, losing −0.26 e. The contributing oxygen states are clearly the 2p states of the four oxygens surrounding the Ti3: O7, O8, O9, and O11. The first small massif of CB between 4 and 4.5 eV is composed only of the $3d_{xy}$ states of Ti1, Ti2, and Ti4 (nonbonding states), followed at 4.5 eV by a higher contribution

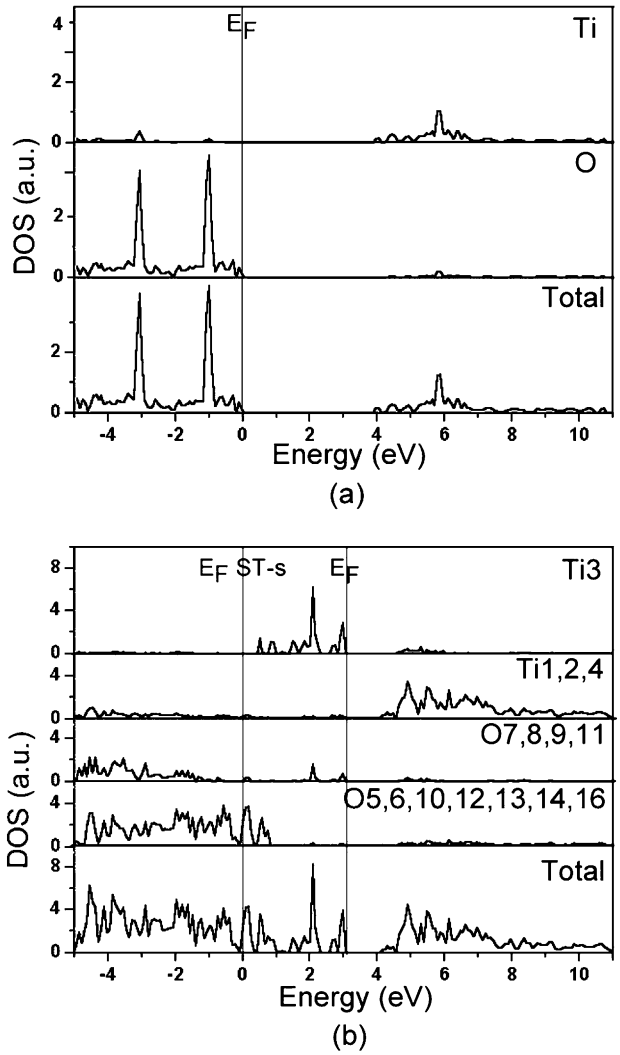

Figure 7. Total and atom-projected DOS for **ST-s** (a) and **ST-d**(b).

of Ti1, Ti2, and Ti4 3d states with a weak participation of Ti3 3d and O 2p states. The Sr 5s states are located between −15 and −18 eV (not shown), more dispersed than in the case of **ST-s**, thus revealing a less ionic interaction with the oxygen ions. The contribution of Sr to the total DOS is weaker than in the **ST-s** case, indicating that the role of the network modifier (Sr) decreases in this deficient crystal. Thus, the suppression of the Sr17 cation weakens the ionic radial interaction between Sr and O, causing the destabilization of the oxygen levels above the top of the VB. In the meantime, the $3d_{xy}$ states of Ti3 are stabilized in the VB by the rupture of the two Ti3−O15 bonds. It is interesting that in another study[42] concerning a comparison of the electronic structure of a crystalline ST and a disordered model in which we had broken the symmetry by displacing the titanium atom we also had created new levels above the VB but they were related only to oxygen states without the contribution of the titanium levels, where major modification consisted of a new splitting of the orbitals in the CB. This result underlines the importance of the Sr network modifier in the electronic structure that acts as a stabilizer for the oxygen contributions.

At this stage of our study, the presence of localized states in the band gap of the structurally disordered and SrO-deficient compound has already been proven, with respect to localized states that are related to the measured optical edges and tails. These results show that the theoretical models are consistent with reality and the interpretation that the exponential optical absorption edge and the optical band gap are controlled by the degree of disorder, structural and thermal, in the lattice of the ST system. This must be related to the Jahn−Teller symmetry-breaking interaction that exists for any set of degenerate electronic states associated with a molecular configuration: molecular distortion is associated with the removal of the electronic degeneracy.[43]

The present study has been completed with the analysis of the Mulliken charges computed for both periodic models, **ST-s** and **ST-d**, in an attempt to understand what in the deficient structure exactly allows the radiative decay leading to PL. Contour and surface plots of the electronic charge density calculated on horizontal selected planes are exhibited in Figure 8, on the left-hand side for **ST-s** and on the right-hand side for

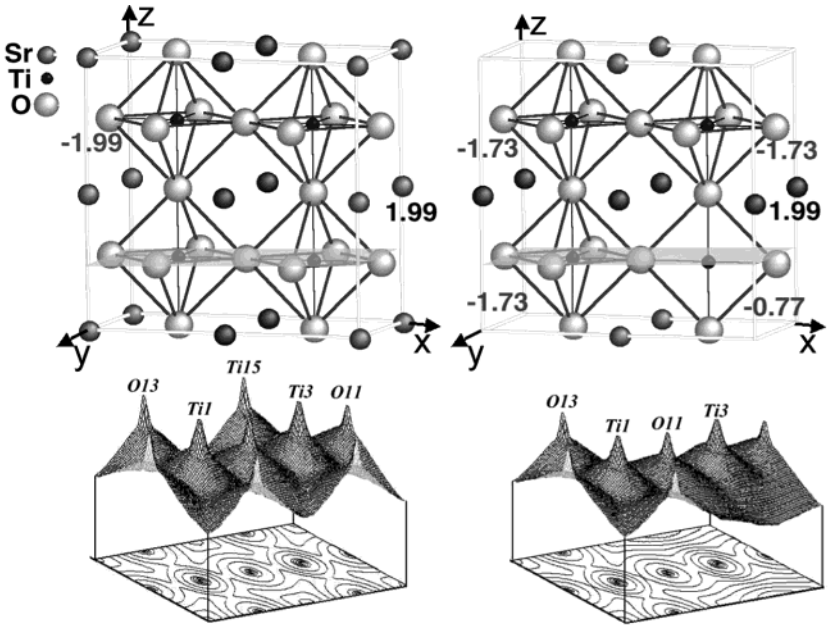

Figure 8. (Top) Mulliken net charges for **ST-s** (left), where $Q_{Sr} = 1.99$ and $Q_{[TiO6]} = -1.99$, and for **ST-d** (right), where $Q_{Sr} = 1.99$, $Q_{[TiO6]} = -1.73$, and $Q_{[TiO4]} = -0.77$. (Bottom) Density of charge contour and surface plots in a horizontal plane cutting Ti1 and Ti3 for **ST-s** (left) and **ST-d** (right).

ST-d. The selected horizontal plane, located at $^1/_4$ of the supercell edge, contains the Ti1 and Ti3 atoms. Figure 8 shows the covalent nature of the Ti−O bond and also emphasizes the fact that the atomic charges are only slightly dependent on the structural deformation. For example, Ti1 net charges are 2.18 e for **ST-s** and 2.16 e for **ST-d**, the more deformation-perturbed atom. Ti3 presents net charges of 2.18 and 1.77 e, respectively, and in turn O7 and O9 are oxidized by 0.26 e each. The charge recombination issued from the symmetry break occurs not only from one metallic center to another but also from the entire cluster formed by the titanium and its surrounding oxygens. The calculated net charges of the four $[TiO_6]$ clusters, −1.99 e, and the four Sr atoms, 1.95 e, are indicated on the upper left side of Figure 8. The corresponding values for the three $[TiO_6]$ clusters, −1.73 e, the $[TiO_4]$ cluster, −0.77 e, and each of the remaining Sr atoms, 1.99 e, of **ST-d** are presented in Figure 7, upper right side. The removal of the Sr17/O15 couple leads to a small decrease in net atomic charge of the $[TiO_6]$ cluster without a notable change in the net charge of the Sr atoms. In addition, this removal creates a weakly charged $[TiO_4]$ cluster, −0.77 e. The charge differential between the $[TiO_4]$ cluster and the three $[TiO_6]$ clusters, about 1 e, allows the system to act as a permanent dipole, encouraging the trapping of holes in the localized states created above the crystalline VB. We think that this is the radiative recombination of the holes with excited electrons that creates the PL properties in these SrO-deficient ST thin films.

In summary, the theoretical results indicate that the formation of a 4-fold oxygen−titanium coordination $[TiO_4]$ through the removal of Sr17 and O15 atoms and the concomitant disappearance of two oxygen−titanium bonds introduces localized electronic levels with O7, O8, O9, and O11 ($2p_x$, $2p_y$, and $2p_z$) character and Ti3 $3d_{xz}$ character above the VB of the structure before deformation (Figure 7b). The **ST-s** structure indeed presents a higher band gap than the **ST-d**, in agreement with the experimental results observed by absorbance spectral data (Figure 3). The coexistence of $[TiO_6]$ and $[TiO_4]$ coordination in the same crystal structure, with different net cluster charges, induces the formation of a charge gradient, allowing the trapping of holes in the new localized electronic levels, and is responsible for the PL behavior.

VI. Conclusions

Thin films of $Sr_{1-x}TiO_{3-x}$ have been synthesized following soft chemical processing, and their structural properties have been obtained by X-ray data, whereas the corresponding PL spectra have been measured. To understand the mechanism of visible PL at room temperature in SrO-deficient $SrTiO_3$, we turned to first-principles calculations as an appropriate tool to rationalize this property. Therefore, we performed quantum-mechanical calculations on crystalline and deficient ST periodic supercell models. From them, we analyzed the electronic structures in terms of DOS, band dispersion, and electronic density contour and surface plots. We used DFT methods with the hybrid, nonlocal B3LYP approximation as implemented in the CRYSTAL98 code.

The knowledge of the geometric structure of ST-deficient thin films provides an essential basis for understanding their PL properties. The analysis of band structure, DOS, and electronic charge density provides keys to the origin of this property. The theoretical results are compared to the experimental data, and an analysis of the calculated electronic structures leads to calculated band gaps that are consistent with the experimentally determined optical gaps.

Moreover, the foresight of localized electronic levels in the deficient-ST structure within the energy band gap of crystalline stoichiometric phase is in accordance with the experimental tail observed in the absorbance spectra of deficient $Sr_{1-x}TiO_{3-x}$. Two main and connected factors are responsible for the PL behavior of SrO-deficient $Sr_{1-x}TiO_{3-x}$:

(i) localized electronic levels induced in the VB by the symmetry-breaking processon going from stoichiometric to deficient $SrTiO_3$, and

(ii) the coexistence of both $[TiO_6]$ and $[TiO_4]$ cluster configurations in the deficient $Sr_{1-x}TiO_{3-x}$ structure yielding a charge imbalance that encourages the trapping of holes in the previously mentioned localized states.

Finally, it is important to remark that the synthetic and experimental methods reported here can be applied to a variety of other perovskite material systems to address a range of open scientific and technological challenges. In addition, computational chemistry has efficiently explained the results of experimental investigation, and the work presented here demonstrates that the joint use of theory and experiment represents a unique opportunity for investigating PL properties in transition-metal oxides.

Acknowledgment. This work was partially supported by the Brazilian research-financing institutions: Fundação de Amparo à Pesquisa do Estado de São Paulo - FAPESP/CEPID, by the Conselho Nacional de Desenvolvimento Científico e Tecnológico - CNPq/PRONEX, and by the Programa de colaboración hispano brasileño no. PHB2001-0040.

References and Notes

(1) Canham, L. T. *Appl. Phys. Lett.* **1990**, *57*, 1046.

(2) Soledade, L. E. B.; Longo, E.; Leite, E. R.; Pontes, F. M.; Lanciotti, F., Jr.; Campos, C. E. M.; Pizani, P. S.; Varela, J. A. *Appl. Phys. A* **2002**, *75*, 629.

(3) Rangel, J. H.; Carreño, N. L. V.; Leite, E. R.; Longo, E.; Campos, C. E. M.; Lanciotti, F., Jr.; Pizani, P. S.; Varela, J. A. *J. Lumin.* **2002**, *99*, 7.

(4) Pizani, P. S.;, Basso, H. C.;, Lanciotti, F.; Boschi, T. M.; Pontes, F. M.; Longo, E.; Leite, E. R. *Appl. Phys. Lett.* **2002**, *81*, 253.

(5) Lanciotti, F.; Pizani, P. S.; Campos, C. E. M.; Leite, E. R.; Santos, L. P. S.; Carreño, N. L. V.; Longo, E. *Appl. Phys. A* **2002**, *74*, 787.

(6) Leite, E. R.; Pontes, F. M. L.; Lee, E. J. H.; Aguiar, R.; Longo, E.; Pontes, D. S. L.; Nunes, M. S. J.; Macedo, H. R.; Pizani, P. S.; Lanciotti, F., Jr.; Boschi, T. M.; Varela, J. A.; Paskocimas, C. A. *Appl. Phys. A* **2002**, *74*, 529.

(7) Leite, E. R.; Santos, L. P. S.; Carreño, N. L. V.; Paskocimas, C. A.; Lanciotti, F., Jr.; Pizani, P. S.; Campos, C. E. M.; Varela, J. A.; Longo, E.; *Appl. Phys. Lett*. **2001**, *78*, 2148.

(8) Leite, E. R.; Pontes, F. M. L.; Paris, E. C.; Paskocimas, C. A.; Lee, E. J. H.; Longo, E.; Pizani, P. S.; Varela, J. A.; Mastelaro, V. *Adv. Mater. Opt. Electron*. **2000**, *10*, 235.

(9) Pontes, F. M.; Leite, E. R.; Longo, E.; Varela, J. A.; Pizani, P. S.; Campos, C. E. M.; Lanciotti, F., Jr. *Adv. Mater. Opt. Electron*. **2000**, *10*, 81.

(10) Pizani, P. S.; Leite, E. R.; Pontes, F. M.; Paris, E. C.; Rangel, J. H.; Lee, E. J. H.; Longo, E.; Delega, P.; Varela, J. A. *Appl. Phys. Lett* **2000**, *77*, 824.

(11) Pinheiro, C. D.; Longo, E.; Leite, E. R.; Pontes, F. M.; Magnani, R.; Varela, J. A.; Pizani, P. S.; Boschi, T. M.; Lanciotti, F. *Appl. Phys. A* **2003**, *77*, 81.

(12) Pontes, F. M.; Pinheiro, C. D.; Longo, E.; Leite, E. R.; De Lazaro, S. R.; Magnani, R.; Pizani, P. S.; Boschi, T. M.; Lanciotti, F., Jr. *J. Lumin*. **2003**, *104*, 175.

(13) Leite, E. R.; Paris, E. C.; Pontes, F. M.; Paskocimas, C. A.; Longo, E.; Pinheiro, C. D.; Varela, J. A.; Pizani, P. S.; Campos, C. E. M.; Lanciotti, F., Jr. *J. Mater. Sci.* **2003**, *38*, 1775.

(14) Pontes, F. M.; Pinheiro, C. D.; Longo, E.; Leite, E. R.; De Lazaro, S. R.; Varela, J. A.; Pizani, P. S.; Boschi, T. M.; Lanciotti, F., Jr. *Mater. Chem. Phys.* **2003**, *78*, 227.

(15) Pontes, F. M.; Longo, E.; Leite, E. R.; Lee, E. J. H.; Varela, J. A.; Pizani, P. S.; Campos, C. E. M.; Lanciotti Jr, F.; Mastellaro, V.; Pinheiro, C. D. *Mater. Chem. Phys.* **2003**, *77*, 598.

(16) Leite, E. R.; Pontes, F. M.; Lee, E. J. H.; Aguiar, R.; Longo, E.; Pontes, D. S. L.; Nunes, M. S. J.; Macedo, H. R.; Pizani, P. S.; Lanciotti, F., Jr.; Boschi, T. M.; Varela, J. A.; Paskocimas, C. A. *Appl. Phys. A* **2002**, *74*, 529.
(17) Pontes, F. M.; Leal, S. H.; Pizani, P. S.; Santos, M. R. M. C.; Leite, E. R.; Longo, E.; Lanciotti, F., Jr.; Boschi, T. M.; Varela, J. A. *J. Mater. Res.* **2003**, *18*, 659.
(18) Blasse, G.; Grabmaier, B. C.; *Luminescent Materials*; Springer-Verlag: Berlin, 1994.
(19) Leonelli, R.; Brebner, J. L. *Phys. Rev. B* **1986**, *33*, 8649.
(20) Eglitis, R. I.; Kotomim, E. A.; Borstel, G. *Eur. Phys. J. B* **2002**, *27*, 483.
(21) Bouma, B.; Blasse, G. *J. Phys. Chem. Solids* **1995**, *56*, 261.
(22) Pontes, F. M.; Longo, E.; Rangel, J. H.; Bernardi, M. I.; E. Leite, R.; Varela, J. A. *Mater. Lett.* **2000**, *43*, 249.
(23) Saunders, V. R.; Dovesi, R.; Roetti, C.; Causa, M.; Harrison, N. M.; Orlando, R.; Zicovich-Wilson, C. M. *CRYSTAL98 User's Manual*; University of Torino: Torino, Italy, 1998.
(24) Lee, C.; Yang, W.; Parr, R. G. *Phys. Rev. B* **1988**, *37*, 785.
(25) Becke, A. D. *J. Chem. Phys.* **1993**, *98*, 5648.
(26) Muscat, J.; Wander, A.; Harrison, N. M. *Chem. Phys. Lett*. **2001**, *42*, 397.
(27) http://www.tcm.phy.cam.ac.uk/~mdt26/crystal.html.
(28) http://www.chimifm.unito.it/teorica/crystal/crystal.html.
(29) Kokalj, A. *J. Mol. Graphics Modell.* **1999**, *17*, 176.
(30) Wood, D. L.; Tauc, J. *Phys. Rev. B* **1972**, *5*, 3144.
(31) Cardona, M. *Phys. Rev. A* **1965**, *140*, 651.
(32) Cohen, M. I.; Blunt, R. F. *Phys. Rev.* **1968**, *168*, 929.
(33) Capizzi, M.; Frova, A. *Phys. Rev. Lett.* **1970**, *25*, 1298.
(34) Blazey, K. W. *Phys. Rev. Lett.* **1971**, *27*, 146.
(35) Noland, J. A. *Phys. Rev.* **1954**, *94*, 724.
(36) Urbach, F. *Phys. Rev.* **1953**, *92*, 1324.
(37) Kahn, A. H.; Leyendecker, A. J. *Phys. Rev. A* **1964**, *135*, 1321.
(38) Mattheis, L. F. *Phys. Rev. B* **1972**, *6*, 4718.
(39) Mo, S. D.; Ching, W. Y.; Chisholm, M. F.; Duscher, G. *Phys. Rev. B* **1999**, *60*, 2416.
(40) O Jones, R.; Gunnarson, O. *Rev. Mod. Phys.* **1989**, *61*, 689.
(41) Heifets, E.; Eglitis, R. I.; Kotomin, E. A.; Maier, J.; Borstel, G. *Surf. Sci.* **2002**, *513*, 211.
(42) Longo, E.; Orhan, E.; Pontes, F. M.; Pinheiro, C. D.; Leite, E. R.; Varela, J. A.; Pizani, P. S.; Boschi, T. M.;Lanciotti, F., Jr.; Beltrán, A.; Andrés, J. *Phys. Rev. B*, in press, 2004.
(43) O'Brien, M. C. M.; Chancey, C. C. *Am. J. Phys.* **1993**, *61*, 688.